5554 *Chem. Mater.* **2010,** *22,* 5554–5562
DOI:10.1021/cm1015614

CHEMISTRY OF MATERIALS
Article

$NaMnFe_2(PO_4)_3$ Alluaudite Phase: Synthesis, Structure, and Electrochemical Properties As Positive Electrode in Lithium and Sodium Batteries

Khiem Trad,[†,‡,§] Dany Carlier,*[,†,‡] Laurence Croguennec,[†,‡] Alain Wattiaux,[†] Mongi Ben Amara,[§] and Claude Delmas[†,‡]

[†]*CNRS, Université de Bordeaux, ICMCB, 87 avenue du Dr. A. Schweitzer, 33608 F-Pessac Cedex, France,* [‡]*CNRS, ENSCBP, ICMCB, 87 avenue du Dr. A. Schweitzer, 33608 F-Pessac Cedex, France, and* [§]*UR: Matériaux Inorganiques, Faculté des Sciences de Monastir, avenue de l'environnement, 5019, Monastir, Tunisia*

Received June 4, 2010. Revised Manuscript Received July 23, 2010

The $NaMnFe_2(PO_4)_3$ alluaudite phase was prepared either by classical solid-state chemistry or by the sol−gel method. Its structure was investigated by Rietveld refinement of XRD and neutron diffraction data in order to precisely determine the cationic distribution. This 3D skeleton structure exhibits two types of 1D tunnels where the Na^+ ions are localized. The material obtained by the sol−gel method exhibits a composition very close to the ideal one, contrary to previous works reported in literature. This study leads us to propose the following formulation for our sample: $(Na_{0.81})_{A(1)}(Na_{0.19})_{A(2)'}(Mn^{II}_{0.87}Fe^{II}_{0.13})_{M(1)}(Fe^{III}_{1.87}Mn^{III}_{0.13})_{M(2)}(PO_4)_3$. The iron/manganese exchange was revealed from neutron data and was supported by Mössbauer spectroscopy (presence of small amount of Fe^{2+} ions in the M(1) type site). The stability of the various Na^+ ions sites within the tunnels were studied by DFT calculations. The intercalation/deintercalation properties of $NaMnFe_2(PO_4)_3$ as positive electrode were tested in lithium and sodium batteries. The cycling curves exhibit a significant polarization even for the material prepared by sol−gel method. For this material, 1.5 Li^+ ions and electrons can be intercalated in the structure at low rate.

Introduction

Since the discovery of highly interesting properties for $LiFePO_4$ as a positive electrode material in lithium ion batteries,[1] the search for novel polyanion-based insertion hosts has been intense.[2−8] In this context, we were interested in an alluaudite type iron manganese sodium phosphate $NaMnFe_2(PO_4)_3$. Richardson reported a preliminary study of some other alluaudite compounds, $Li_{0.75}Na_{0.25}MnFe_2(PO_4)_3$, $Na_2FeMn_2(PO_4)_3$, and $LiNaFeMn_2(PO_4)_3$,[9] that exhibit poor electrochemical activities. The alluaudite structure was first determined on natural minerals in 1955 by Fisher,[10] who showed that alluaudite compounds crystallize in the monoclinic $C2/c$ space group. Moore in 1971[11] proposed the general formula $X(2)X(1)M(1)M(2)_2(PO_4)_3$, in which X and M cations are written according to decreasing size. The structure consists of infinite chains (Figure 1a) formed by a succession of M(2) octahedral pairs linked by highly distorted M(1) octahedra (shown also by hatched polyhedra in Figure 1c). Equivalent chains are connected by phosphate tetrahedra to form sheets oriented perpendicular to [010] (Figure 1b). Equivalent sheets are hold together by PO_4 tetrahedra to form a three-dimensional architecture with two sets of tunnels in the c direction: tunnel 1 (1/2, 0, z) and tunnel 2 (0, 0, z) (Figure 1c). More recently, instead of Moore's X(1) and X(2) labels for the sites located in these two tunnels, Leroux et al.[12] and Hatert et al.[13] proposed a new general formula for the alluaudite structure in order to take into account the different sites available in the tunnels: $[A(2)A(2)'][A(1)A(1)'A(1)'']M(1)M(2)_2(PO_4)_3$, where A(2) and A(2)′ sites are located in tunnel 2 and A(1), A(1)′, and A(1)″ sites are located in tunnel 1. Whereas the M sites must be filled, the A sites in the tunnels could be empty or partially occupied. Among the large

*Corresponding author. Phone: +33 (0) 5 40 00 31 75. Fax: +33 (0) 5 40 00 27 61. E-mail: carlier@icmcb-bordeaux.cnrs.fr.

(1) Padhi, A. K.; Nanjundaswamy, K. S.; Goodenough, J. B. *J. Electrochem. Soc.* **1997**, *144*, 1188–1194.
(2) Barker, J.; Gover, R. K. B.; Burns, P.; Bryan, A. *Electrochem. Solid-State Lett.* **2005**, *8*, A285–A287.
(3) Nyten, A.; Abouimrane, A.; Armand, M.; Gustafsson, T.; Thomas, J. O. *Electrochem. Commun.* **2005**, *7*, 156–160.
(4) Kishore, M. S.; Pralong, V.; Caignaert, V.; Varadaraju, U. V.; Raveau, B. *Electrochem. Commun.* **2006**, *8*, 1558–1562.
(5) Ji, X. L.; Lee, K. T.; Nazar, L. F. *Nat. Mater.* **2009**, *8*, 500–506.
(6) Recham, N.; Chotard, J.-N.; Dupont, L.; Delacourt, C.; Walker, W.; Armand, M.; Tarascon, J.-M. *Nat. Mater.* **2010**, *9*, 68–74.
(7) Recham, N.; Chotard, J.-N.; Jumas, J.-C.; Laffont, L.; Armand, M.; Tarascon, J.-M. *Chem. Mater.* **2010**, *22*, 1142–1148.
(8) Marx, N.; Croguennec, L.; Carlier, D.; Bourgeois, L.; Kubiak, P.; Cras, F. L.; Delmas, C. *Chem. Mater.* **2010**, *22*, 1854–1861.
(9) Richardson, T. J. *J Power Sources* **2003**, *119−121*, 262–265.
(10) Fisher, D. J. *Am. Mineral.* **1955**, *40*, 1100.
(11) Moore, P. B. *Am. Mineral.* **1971**, *56*, 1955.
(12) Leroux, F.; Mar, A.; Guyomard, D.; Piffard, Y. *J. Solid State Chem.* **1995**, *117*, 206–212.
(13) Hatert, F.; Keller, P.; Lissner, F.; Antenucci, D.; Fransolet, A.-M. *Eur. J. Mineral.* **2000**, *12*, 847–857.

Published on Web 09/13/2010

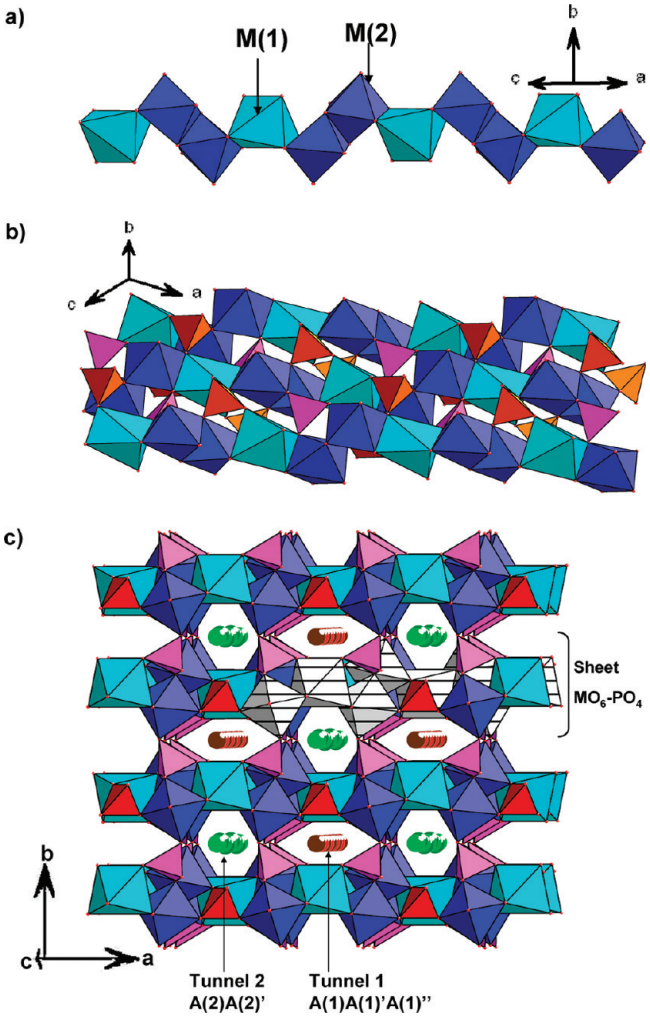

Figure 1. (a) View of the chain showing the distorted octahedra M(1) and M(2) sites. (b) View of the sheet constituted by MO_6 octahedra and PO_4 tetrahedra. (c) View of the alluaudite structure in the *ab* plane. The hatched polyhedra represent a MO_6 octahedra chain parallel to the [101] direction.

variety of phosphate and arsenate alluaudite compounds, we were interested in an iron manganese sodium phosphate $NaMn^{II}Fe^{III}_2(PO_4)_3$, which exhibits a theoretical total capacity close to that of $LiFePO_4$ (~170 mA h/g) if it could be cycled between the end members $Mn^{III}Fe^{III}_2(PO_4)_3$ and $Na(Na,Li)_2Mn^{II}Fe^{II}_2(PO_4)_3$. In the literature, several structural studies deal with natural or synthetic alluaudite compounds, but with compositions that differ significantly from $NaMnFe_2(PO_4)_3$. Moore studied the natural one, which was later reinvestigated, leading to the following formulation $(Na_{0.76}Ca_{0.4})(Mn_{1.04})(Fe_{1.73}Al_{0.21}Mg_{0.04})(PO_4)_3$,[14] and then Hatert et al. reported the study of the synthetic $Na_{1.304}Mn_{0.968}Fe_{1.9}(PO_4)_3$ and $Na_{0.89}Mn_{1.25}Fe_{1.95}(PO_4)_3$ phases.[13,15,16] To the best of our knowledge, no structural characterization of the stoichiometric $NaMnFe_2(PO_4)_3$ has been reported. In this paper, we report a new route for the synthesis of $NaMnFe_2(PO_4)_3$ as powder, the study of its structure by X-ray and neutron diffraction techniques as well as Mössbauer spectroscopy, supported by ab initio calculations. Finally, we will present the cycling performances of $NaMnFe_2(PO_4)_3$ used as positive electrode in sodium and lithium cells in comparison with those of a sample prepared by the classical solid-state route.

(14) Redhammer, G. J.; Tippelt, G.; Bernroider, M.; Lottermoser, W.; Amthauer, G.; Roth, G. *Eur. J. Mineral.* **2005**, *17*, 915–932.
(15) Hermann, R. P.; Hatert, F.; Fransolet, A.-M.; Long, G. J.; Grandjean, F. *Solid State Sci.* **2002**, *4*, 507–513.
(16) Hatert, F.; Long, G. J.; Hautot, D.; Fransolet, A.-M.; Delwiche, J.; Hubin-Franskin, M. J.; Grandjean, F. *Phys. Chem. Miner.* **2004**, *31*, 487–506.

Experimental Section

As $NaMnFe_2(PO_4)_3$ will be studied as a positive electrode material in batteries, the powder morphology is important since smaller grain size can significantly improve the intercalation and deintercalation kinetic and in turn the cell capacity. Several synthesis conditions were explored in order to get compounds with the smallest particle size, for comparison we will report here only two of them. Method A: we first tried the solid-state reaction carried out at 900 °C as reported in the literature,[13] but with a shorter heating thermal treatment. A mixture of Na_2CO_3 (pure, Riedel-de Haën), $MnCO_3$ (99.9%, Aldrich), $FeC_2O_4.2H_2O$ (pure, Prolabo), and $(NH_4)H_2PO_4$ (98.5%, Sigma Aldrich) was dissolved in a beaker filled with a diluted nitric acid solution and then evaporated by heating. The residual powder was thermal-treated under air, successively for 6 h at 400 °C and 6 h at 600 °C, with an intermediate grinding between each thermal treatment, and then quenched in air after 30 min at 900 °C. Method B: $NaMnFe_2(PO_4)_3$ compound was also synthesized via the Pechini method. Stoichiometric amounts of Na_2CO_3, $MnCO_3$, $FeC_2O_4 \cdot 2H_2O$, and $(NH_4)H_2PO_4$ were mixed in distilled water with sufficient nitric acid added for total dissolution (few drops), in which citric acid was added as a complexing agent. The solution was heated under vigorous stirring until evaporation of water, leading to the formation of a viscous gel. The as-formed gel was further heated until decomposition of the organic compounds, and a spontaneous exothermic reaction occurred, resulting in the formation of a black fine powder that was ground and introduced in a furnace already at 800 °C for 30 min in air atmosphere. Green fine powder was obtained by quenching finally the product in air.

The particle morphology was characterized by scanning electron microscopy (SEM) using an emission field microscope Hitachi S-450. The powders were metallized by gold−palladium plasma.

To confirm the chemical composition of the sample, the Na/P, Mn/P, and Fe/P ratios were determined using an ICP-OES spectrometer (Varian 720-ES Optical Emission Spectrometer) after complete dissolution of the powder into a hydrochloric acid solution. For both samples, the Na/P, Mn/P, and Fe/P ratios are really close to those of the target composition. For example, ICP measurements for the sample prepared by method B lead to the $Na_{0.95(5)}Mn_{1.09(5)}Fe_{2.02(5)}(PO_4)_3$ chemical formula. To the best of our knowledge, this is the first time that a synthetic alluaudite phase is obtained so close from the ideal $NaMnFe_2(PO_4)_3$ stoichiometry.

The X-ray diffraction patterns were collected using a PANalytical X'pert Pro diffractometer (Cu Kα1 radiation, antiscatter slit of 1/2° and divergence slit of 1° on the incident beam path). They were recorded in the [5−120]° (2θ) angular range using an 0.0167° (2θ) step and a constant counting time of 10 s. Neutron diffraction was performed at the Laue Langevin Institute (ILL) in Grenoble (France) on the high-resolution two-axis powder diffractometer D2B. The diffraction pattern was collected in transmission mode at room temperature with a wavelength of

1.5944(4) Å. The sample was contained in an 8 mm diameter vanadium tube. The pattern was recorded in the [0−160]° angular range using a 0.05° (2θ) step with an accumulation time of 4 h. Because of the geometry of the neutron diffractometer, it was necessary to correct the absorption in order to take into account a decrease in the experimental diffracted intensity compared to the expected one. The calculated absorption correction coefficient (μR factor in the FullProf program) is equal to 0.141 for $NaMnFe_2(PO_4)_3$. μ is the linear absorption coefficient of the sample and is defined as $\mu = \frac{n}{V}\sum n_i\sigma_i$, where n is the number of formula units in the unit cell, V the cell volume, n_i the number of a given atom in the formula unit, and σ_i the sum of coherent and incoherent scattering cross sections for the atom i. R is the radius of the vanadium cylinder. The X-ray and neutron diffraction patterns were analyzed by the Rietveld method as implemented in the Fullprof program.[17]

Mössbauer spectroscopy has been used to study the iron oxidation state and coordination. The experiments were performed at room temperature in transmission geometry with a constant acceleration spectrometer using ^{57}Co source in a Rh matrix. The velocity was calibrated by using pure iron metal as standard material at room temperature. All isomer shifts reported in this work refer to the natural α-Fe at 293 K. All the spectra were recorded in a large range of velocity (− 10 mm/s; + 10 mm/s) and show the absence of magnetic impurities in the sample and especially of α-Fe_2O_3, which is magnetic at room temperature. The fraction of iron present in the structure was determined assuming equal recoil-free factor (f) for each of the ^{57}Fe nuclei in the structure.

First-principles calculations were performed using density functional theory (DFT) in the Generalized Gradient Approximation GGA (PBE)[18] and GGA+U with the Projector Augmented Wave (PAW) method[19] as implemented in the Vienna Ab Initio Simulation Package (VASP).[20] A plane wave cutoff energy of 500 meV and a 2 × 2 × 2 k-points grid were used for all cells in order to get the total energy converged by less than 5 meV/unit cell. The structures were relaxed and the final energies of each optimized geometry were recalculated so as to correct for changes in basis during relaxation. Previous studies showed that the GGA method allows a better simulation of magnetic interactions and Jahn−Teller distortions than LDA method.[21] The DFT+U method allows for more accurately treating the electronic structure of strongly correlated systems and was shown to be particularly adapted to treat the transition metal phosphates and recover the experimental average voltages[22] and to show the existence of the two phases domain in the $FePO_4$/$LiFePO_4$ system.[23] In our study, Dudarev's approach was used in order to perform GGA + U calculations. In this method, the parameters U ("on site" electron−electron repulsion) and J (exchange interaction) are not entered separately as only the difference ($U - J$) is meaningful. It therefore allows us to consider a single parameter that will be called $U_{eff} = U - J$. Recently, Zhou et al. developed a method to evaluate by ab initio the U value[22] for a given exchange J value. In our study, we therefore used the U_{eff} values such determined for H.S. Fe^{3+} and Mn^{2+} ions in the olivine MPO_4 type phase,[22] i.e., U_{eff} = 4.9 eV for H.S. Fe^{3+} and U_{eff} = 3.92 eV for H.S. Mn^{2+}. As our magnetic measurements (not shown here, but in agreement with the presence of HS-Fe^{3+} and HS-Mn^{2+} in octahedral site in $NaMnFe_2(PO_4)_3$) did not reveal any magnetic transition at low temperature, we chose to perform the calculations in the ferromagnetic configuration.

For the evaluation of its electrochemical performance in laboratory sodium and lithium cells, $NaMnFe_2(PO_4)_3$ was first ball-milled for 15 min with a (1:1) mixture of carbon black and graphite, and then PVDF (polyvinylidene fluoride) was added as binder. The final composition of the positive electrode was approximately 80 wt % active material, 15 wt % carbon black/graphite (1:1), and 5 wt % PVDF. Some drops of *N*-methyl pyrrolidone (NMP) were added to get a fluid mixture. The carbon content from 10 to 20 wt % does not affect the cycling properties; however, the ball milling step was essential to improve the material capacities. The resulting slurry was spread uniformly onto an aluminum foil, and then dried, pressed, and cut into disks that were dried under a vacuum at 100 °C overnight. Metallic sodium or metallic lithium were used as negative electrodes and $NaClO_4$ in PC (1 M) or $LiPF_6$ (1 M) in a mixture of ethylene carbonate (EC), propylene carbonate (PC), and dimethyl carbonate (DMC) in volume proportions 1:1:3 were used as electrolytes. The batteries were assembled in an argon-filled drybox ([H_2O] < 3 ppm) and cycled at room temperature in galvanostatic mode at a constant C/100 rate or C/50 rate (corresponding to a theoretical exchange of one electron per formula during a charge or a discharge in 100 or 50 h). The electrochemical tests were carried out with a homemade apparatus or with a Biologic VMP1 system.

Results and Discussions

3.1. Structural Characterization. The experimental XRD patterns of the samples prepared by the two methods are really similar and could be indexed using the monoclinic $C2/c$ space group expected for the alluaudite structure. Figure 2 shows the XRD pattern of the sample prepared by method B. The XRD pattern refinement with the Le Bail method[24] led to quite similar cell parameters for the two samples [a = 12.0269(1) Å, b = 12.5490(1) Å, c = 6.4169(2) Å, and β = 114.17(3)° for the sample prepared by method A and a = 11.9878(2) Å, b = 12.5364(2) Å, c = 6.3980(1) Å, and β = 114.22(1)° for the sample prepared by method B] which are of the same order of magnitude than those reported for natural and synthetic alluaudites,[13,16] although for those latter their compositions differ significantly from the $NaMnFe_2(PO_4)_3$ stoichiometry. Note that a very small quantity of quartz α-$FePO_4$ as impurity was detected by XRD in the two samples (only the (102) peak of $FePO_4$ was detected at 25.8°(2θ) and indicated by * in Figure 2). In the following, in agreement with the results of the chemical analyses and the negligible amount of $FePO_4$, the formulas of the studied materials are considered to be the nominal ones. We report here the full structural study from XRD and neutron diffraction experiments performed on the $NaMnFe_2(PO_4)_3$ sample prepared by method B. The analysis of the XRD pattern allowed us to determine the cell parameters and the Na ion sites by calculating Fourier

(17) T. Roisnel, J. R.-C. *Mater. Sci. Forum* **2001**, *378−381*, 118–123.
(18) Perdew, J. P.; Burke, K.; Ernzerhof, M. *Phys. Rev. Lett.* **1996**, *77*, 3865.
(19) Kresse, G.; Joubert, D. *Phys. Rev. B* **1999**, *59*, 1758.
(20) Kresse, G.; Furthmüller, J. *Phys. Rev. B* **1996**, *54*, 11169.
(21) Mishra, S. K.; Ceder, G. *Phys. Rev. B* **1999**, *59*, 6120.
(22) Zhou, F.; Cococcioni, M.; Marianetti, C. A.; Morgan, D.; Ceder, G. *Phys. Rev. B* **2004**, *70*, 235121.
(23) Zhou, F.; Maxisch, T.; Ceder, G. *Phys. Rev. Lett.* **2006**, *97*, 155704.
(24) Bail, A. L.; Duroy, H.; Fourquet, J. *Mater. Res. Bull.* **1988**, *23*, 447–452.

difference maps considering the Mn and Fe transition metal ions in the M(1) and M(2) sites, respectively. For the Rietveld refinement, the total amount of Na^+ ions in the structure was constraint to one in agreement with the chemical analyses and the 4e M(1) and 8f M(2) sites were constraint to be fully occupied. Figure 2 shows the comparison of the experimental and calculated XRD patterns. A good minimization of the difference is observed with small reliability factors. In agreement with the literature, the sodium ions were found to partially occupy the A(1) and A(2)′ sites located, respectively, in tunnels 1 and 2 of the structure. The description of these sites will be given in the following. The possibility for the presence of

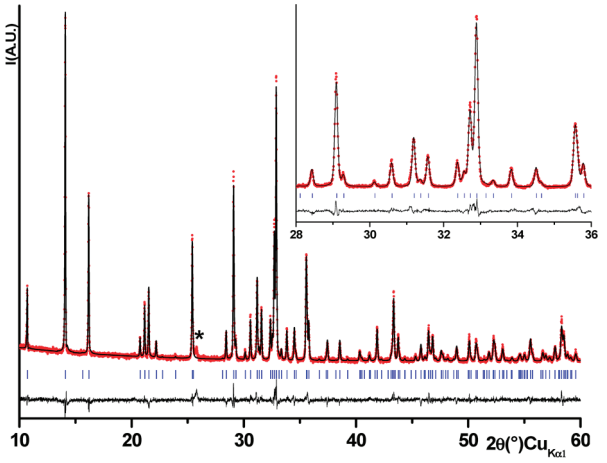

Figure 2. Comparison of the experimental and calculated X-ray diffraction patterns of $NaMnFe_2(PO_4)_3$ prepared by method B. Enlargement of the plot in the 28−36° (2θ) range is given in the inset. The impurity $FePO_4$ is indicated with *.

transition metal ions in the tunnels sites was also tested, but excluded from our XRD Rietveld refinement. Neutron diffraction technique was then used in order to distinguish iron and manganese atoms that exhibit close X-ray scattering atomic factors, but very different (in magnitude and sign) Fermi lengths (b(Fe) = 0.945×10^{-12} cm and b(Mn) = -0.373×10^{-12} cm). The Rietveld refinement of the neutron diffraction data was thus carried out taking into account the results obtained from the XRD data refinement and analyzing Fourier difference maps in order to investigate a possible exchange between Mn/Fe sites. In a first step, Mn and Fe atoms were placed only, respectively in M(1) and M(2) sites: the Fourier difference map showed a positive residual nuclear density in the M(1) site position and a negative one in the M(2) site, which were attributed respectively to the presence of a small amount of iron in M(1) and of manganese in M(2). In a second step, the occupancy factors of the two transition metal ions in the two sites were refined simultaneously assuming that the M(1) and M(2) sites were fully occupied according to the stoichiometry Mn/Fe = 1/2. It appears that Mn and Fe ions are mainly located respectively in M(1) and M(2) sites, but with an exchange of 0.13 between M(1) and M(2) (Table 1). Figure 3 shows the resulting calculated neutron diffraction pattern in comparison with the experimental one. The good quality of the refinement shown by the small difference and small reliability factors suggests the adequacy of the structural model to describe the structure of $NaMnFe_2(PO_4)_3$. Table 1 gives the refined parameters obtained after the Rietveld refinement of the neutron diffraction data and Table 2 gives the resulting Na−O, M−O, and P−O distances.

Table 1. Profile and Structural Parameters Determined by the Rietveld Refinement of the Experimental Neutron Diffraction Pattern of $NaMnFe_2(PO_4)_3$ Prepared by Method B; Thermal Coefficients Were Fixed to 1 for Sodium Atoms and 0.8 for All the Other Atomsa

atom	site	Wyckoff position			occupancy
Na(1)	A(1) 4b	1/2	0	0	0.815(1)
Na(2)	A(2)′ 4e	0	0.022(6)	1/4	0.185(1)
Mn(1)	M(1) 4e	0	0.261(2)	1/4	0.870(3)
Fe(2)	M(1) 4e	0	0.261(2)	1/4	0.130(3)
Fe(1)	M(2) 8f	0.219(3)	0.151(3)	0.129(7)	0.935(3)
Mn(2)	M(2) 8f	0.219(3)	0.151(3)	0.129(7)	0.065(3)
P(1)	4e	0	−0.285(6)	1/4	1
P(2)	8f	0.242(5)	−0.108(6)	0.130(1)	1
O(1)	8f	0.454(5)	0.714(5)	0.532(2)	1
O(2)	8f	0.098(5)	0.640(8)	0.241(2)	1
O(3)	8f	0.329(5)	0.663(5)	0.103(1)	1
O(4)	8f	0.119(5)	0.396(4)	0.311(1)	1
O(5)	8f	0.224(5)	0.822(4)	0.316(1)	1
O(6)	8f	0.312(5)	0.502(3)	0.374(1)	1

Conditions of the Run	
wavelength	1.5944(4) Å
temperature	293 K
angular range	$0° \le 2\theta \le 160°$
step scan increment (2θ)	0.05°
sample displacement (2θ)	0.04(1)°
profile parameters (pseudo-Voigt Function)	η = 0.28(2) U = 0.49(3) V = −0.61(3) W = 0.29(3)
conventional Rietveld R factors	R_{wp} = 12.3%; R_B = 6.7%; Scor = 2.4

[a] Theoretical composition $NaMnFe_2(PO_4)_3$; space group $C2/c$; a = 11.9878(2) Å, b = 12.5364(2) Å, c = 6.3980(1) Å, β = 114.22(1)°, V = 876.88(4) Å^3; Constraints: nNa(1) + nNa(2) = 1; nMn(1) + nFe(2) = 1; nFe(1) + nMn(2) = 1.

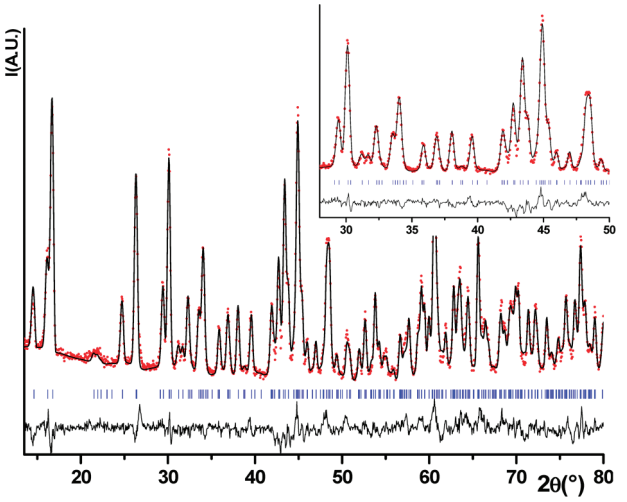

Figure 3. Comparison of the experimental and calculated neutron diffraction patterns of $NaMnFe_2(PO_4)_3$ prepared by method B. Enlargement of the plot in the range 28−50° (2θ) is given in the inset.

Table 2. Selected Interatomic Distances (Å) Determined for $NaMnFe_2(PO_4)_3$ from the Rietveld Refinement of the Neutron Diffraction Dataa

M(1)−O(1) = 2.17(1) Å ×2	M(2)−O(1) = 2.06(1) Å
M(1)−O(3) = 2.23(1) Å ×2	M(2)−O(2) = 1.99(1) Å
M(1)−O(4) = 2.14(1) Å ×2	M(2)−O(3) = 2.02(1) Å
⟨M(1)−O⟩ = 2.18 Å	M(2)−O(5) = 2.05(1) Å
Δ M(1) = 2.94×10^{-4}	M(2)−O(5) = 2.24(1) Å
∑BV (Mn^{2+}) = 2.07 with r_0 = 1.79 Å	M(2)−O(6) = 1.90(1) Å
∑BV (Fe^{2+}) = 1.78 with r_0 = 1.734 Å	⟨M(2)−O⟩ = 2.05 Å
∑BV(Fe^{3+}) = 1.90 with r_0 = 1.759 Å	ΔM(2) = 2.44×10^{-3}
≥ Mn^{2+} and Fe^{2+} in M(1) site	∑BV(Fe^{3+}) = 2.85 with r_0 = 1.759 Å
	∑BV(Mn^{3+}) = 2.85 with r_0 = 1.76 Å
	∑BV (Mn^{2+}) = 3.12 with r_0 = 1.79 Å
	≥ Fe^{3+} and Mn^{3+} in M(2) site
P(1)−O(1) = 1.55(1) Å ×2	P(2)−O(3) = 1.54(1) Å
P(1)−O(2) = 1.51(2) Å ×2	P(2)−O(4) = 1.55(1) Å
⟨P(1)−O⟩ = 1.53 Å	P(2)−O(5) = 1.55(1) Å
	P(2)−O(6) = 1.53(2) Å
	⟨P(2)−O⟩ = 1.54 Å
Na(1)−O(2) = 2.31(1) Å ×2	Na(2)−O(3) = 2.57(1) Å ×2
Na(1)−O(4) = 2.56(1) Å ×2	Na(2)−O(6) = 2.69(1) Å ×2
Na(1)−O(4) = 2.32(1) Å ×2	Na(2)−O(6) = 2.54(1) Å ×2
⟨Na(1)−O⟩ = 2.4 Å	⟨Na(2)−O⟩ = 2.6 Å

[a] The polyhedra distortion is calculated with the formula $\Delta = \frac{1}{N}\sum_{i=1}^{N}\left(\frac{d_i - \langle d\rangle}{\langle d\rangle}\right)^2$, where d_i is the length of the bond i, $\langle d\rangle$ the M−O bonds' average length, and N the number of lengths. ΣBV is the bond valence sum calculated using the Brown method by means of the equation $BV = e^{r_0 - r/0.37}$,[32] where r is the bond length and r_0 is the bond-valence parameter corresponding to each Mn^{n+} cation.

Na^+ Sites. In synthetic and natural alluaudite family,[25−27,16,28] sodium ion appeared to be a very common element, its relatively large ionic radius (1.02 Å) gives it the possibility, depending on the composition, to be distributed over the large A sites in the tunnels but also in the M(1) site.[29] Studies of alluaudite sodium phosphates and arsenates show that the sodium ions are generally localized preferentially in the A(1) and A(2)′ sites. In our case and according to the diffraction data, sodium ions were localized in two different crystallographic sites: Na(1) in A(1) and Na(2) in A(2)′. The occupancy factors given in Table 1 indicate that the A(1) site is predominant (0.81 Na^+ in A(1)(1/2,0,0) and 0.19 Na^+ in A(2)′(0,0.022(6),1/4)). Figure 4 shows the polyhedral environments of the sodium ions. The A(1) site is a distorted octahedral site and the A(2)′ site is a distorted prismatic site (see Table 2 for the Na−O distances). Two other oxygen ions are located at 2.97 Å from A(1) and two at 3.18 Å from A(2)′, but were not considered in our case to be part of the coordination polyhedron.

The sodium sites stability in the $NaMnFe_2(PO_4)_3$ was investigated theoretically by GGA and GGA+U calculations. The structural model considered in these calculations was the "ideal" one, i.e., $NaMnFe_2(PO_4)_3$ with no Mn/Fe site exchange. In the calculations, the sodium ion was considered to fully occupy one of the A sites reported by Hatert et al.[13] The four following hypothesis were considered A(1)(4b)(1/2,0,0), A(1)′(4e)(0,∼0.5,1/4), A(2)-(4a)(0,0,0) and A(2)′(4e)(0,∼0,1/4). All structures were then fully relaxed. In both GGA and GGA+U calculations, the most stable structure was found with all Na^+ ions located in the A(1) site. Therefore, the energy of this structure was taken as reference energy. In Figure 5, the energy of the other structures are represented by their difference from our reference energy and expressed per $NaMnFe_2(PO_4)_3$ formula unit. Despite some differences in the gaps between energies calculated with GGA or GGA+U methods, the relative sites stability obtained with the two calculation methods is the same. The two sites considered in tunnel 1, i.e., A(1) and A(1)′, are more stable than the two sites considered in tunnel 2, A(2) and A(2)′, A(1) being more stable than A(1)′ and A(2)′ being more stable than A(2). The relative site stability found theoretically is in agreement with the experimental results that give the A(1) site as the mainly occupied one. Note that A(1) and A(1)′ are the two most stable sites but adjacent sites cannot be occupied simultaneously because of a very short Na−Na distance (experimentally, 1.6 Å). Experimentally, around 0.19 Na^+ ions were also found in A(2)′, which is theoretically the most stable site of tunnel 2 (Figure 5). We therefore performed calculations placing 0.25 Na^+ ions in A(2)′ and 0.75 Na^+ ions in A(1). As seen in Figure 5, this configuration is not more stable than the one with all Na^+ ion in A(1) site. The presence of Na^+ ions in A(2)′ is therefore not yet understood but was shown to be independent of the Fe/Mn site exchange ratio (discussed in a forthcoming paper). The optimized structural parameters calculated for the structures with all Na^+ ions in A(1) sites or 0.25 Na^+ ions in A(2)′ and 0.75 Na^+

(25) Antenucci, D.; Miehe, G.; Tarte, P.; Schmahl, W. W.; Fransolet, A.-M. *Eur J Mineral* **1993**, *5*, 207–213.
(26) Hatert, F.; Antenucci, D.; Fransolet, A.-M.; Liégeois-Duyckaerts, M. *J. Solid State Chem.* **2002**, *163*, 194–201.
(27) Hidouri, M.; Lajmi, B.; Wattiaux, A.; Fournés, L.; Darriet, J.; Amara, M. B. *J. Solid State Chem.* **2004**, *177*, 55–60.
(28) Hatert, F. *Acta Crystallogr., Sect C* **2006**, *C62*, i1–i2.
(29) Khorari, S.; Rulmont, A.; Tarte, P. *J. Solid State Chem.* **1997**, *134*, 31–37.

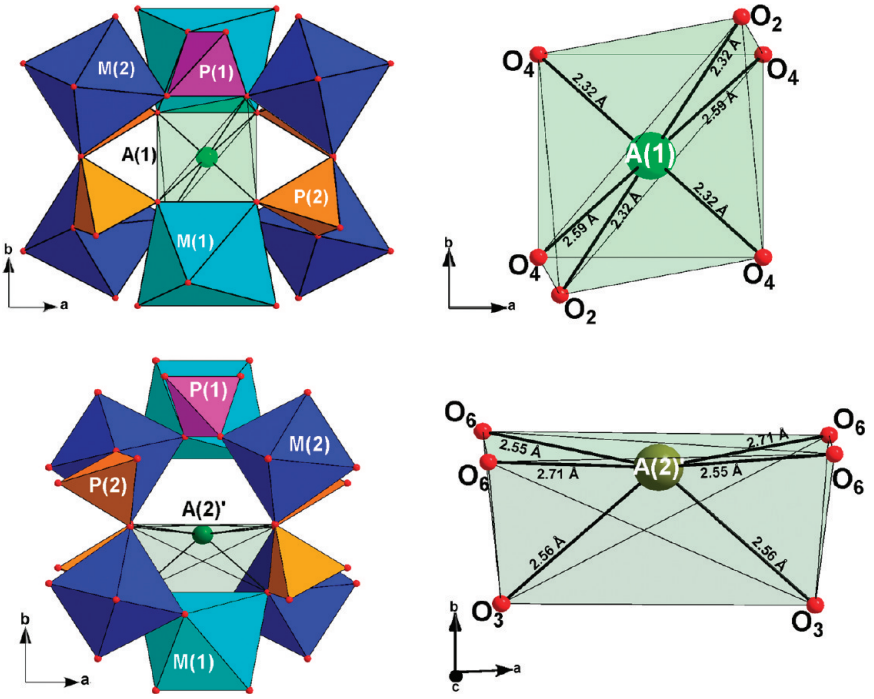

Figure 4. Local environments determined from the Rietveld refinement of XRD and neutron diffraction data for the sodium Na(1) and Na(2) in the A(1) and A(2)′ crystallographic sites, respectively.

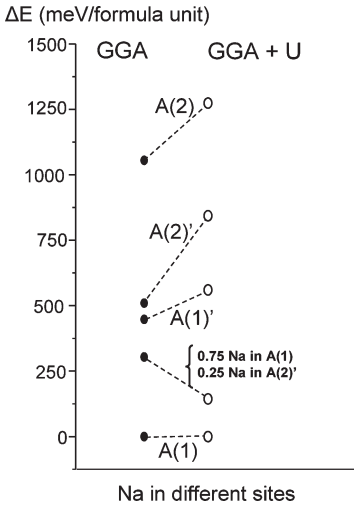

Figure 5. Investigation by GGA and GGA+U calculations of the theoretical sodium stability in the different available sites in the tunnels of the $NaMnFe_2(PO_4)_3$ structure. The sodium ions were considered to fully occupy each of the A sites reported by Hatert et al.,[13] A(1)(1/2,0,0), A(1)′(0,∼0.5,1/4), A(2)(0,0,0), and A(2)′(0,∼0,1/4); or to partially occupy A(1) and A(2)′ sites. The energies of these structures are given relatively to that of the most stable structure, i.e., with all Na in A(1) and expressed per $NaMnFe_2(PO_4)_3$ formula unit.

ions in A(1) are given in Table 3 in comparison with our experimental parameters. The optimized cell parameters of the lattice structure are pretty close to the experimental ones, whatever the calculation method used, and the Na−O distances for the two sites are in good agreement with those determined from our experimental data refinements.

Fe/Mn Site Exchange. From our experimental XRD and neutron data refinements, we observed some Mn/Fe exchange between the M(1) and M(2) sites (a and b, respectively Figure 6). Such transition metals exchange between the M sites was already reported for $NaMnIn_2(PO_4)_3$,[30] where Mn and In are present in both M(1) and M(2) sites. According to their sizes, the M(2) site is more suitable for smaller ions as HS-Fe^{3+} (0.64 Å[31]), whereas the M(1) site is more suitable for larger ions such as HS-Mn^{2+} (0.82 Å[31]). Therefore, the oxidation state of the iron and manganese ions located respectively in the M(1) and M(2) sites because of the cation exchange is not clear. We undertook Mössbauer spectroscopy measurements in order to investigate the oxidation state of the iron ions in $NaMnFe_2(PO_4)_3$. The general profile of the Mössbauer spectra obtained indicates that it should be fitted with two quadrupolar doublets, a predominant one with a small isomer shift and a quadrupole splitting assigned to Fe^{3+} ions with a high-spin configuration and located in octahedral environments as expected from the structure (M(2) site), and a minor one with a large isomer shift and a quadrupole splitting assigned to Fe^{2+} ions located in octahedral sites. As the experimental lines are pretty broad, the Mössbauer spectrum was fitted by considering a distribution of quadrupolar splittings (linked to a distribution of local iron environments) with the full width at half-maximum (Γ) being fixed to the expected value of Γ = 0.25 mm/s. Figure 6c shows the experimental Mössbauer spectra recorded for $NaMnFe_2(PO_4)_3$ prepared by method B in comparison with the fitted one. The characteristic parameters deduced from this refinement, the isomer shift (δ) and the quadrupole splitting (Δ) are given in Table 4. The spectrum exhibits thus 2 doublets with isomer shifts of 0.43 and 1.22 mm/s, which confirm the presence of 2

(30) Hatert, F.; Hermann, R. P.; Long, G. J.; Fransolet, A. M.; Grandjean, F. *Am. Mineral.* **2003**, *88*, 211–222.
(31) Shannon, R. D.; Prewitt, C. T. *Acta Crystallogr., Sect. B* **1969**, *25*, 925–946.

Table 3. Comparison of the Optimized Structural Parameters Obtained for $NaMnFe_2(PO_4)_3$ with the GGA and GGA+U Calculation Methods Depending on the Sites Occupied by Sodium Ions

	all Na^+ in A(1) (1/2,0,0) most stable site		all Na^+ in A(2)′(0,0.022(6),1/4)		0.75 A(1) (1/2,0,0) + 0.25 A(2)′(0,0.022(6),1/4)		0.815(2)A(1) (1/2,0,0) + 0.185(2)A(2)′(0,0.022(6),1/4)
	GGA	GGA+U	GGA	GGA+U	GGA	GGA+U	experimental
a (Å)	11.933	12.103	11.742	12.014	11.880	12.069	11.9878(2)
b (Å)	12.675	12.617	12.378	12.378	12.588	12.604	12.5364(2)
c (Å)	6.548	6.467	6.692	6.503	6.530	6.465	6.3980(1)
β (deg)	114.59	113.94	115.21	114.06	114.52	113.94	114.22(1)
V (Å^3)	900.7	902.5	879.9	883.1	888.40	898.93	876.88(4)
*d*Na(1)−O (Å)	2.34 ×2	2.34 ×2			2.30 ×2	2.31 ×2	2.31(1) ×2
	2.44 ×2	2.35 ×2			2.38 ×2	2.34 ×2	2.32(1) ×2
	2.60 ×2	2.56 ×2			2.49 ×2	2.51 ×2	2.56(1) ×2
*d*Na(2)−O (Å)			2.32 ×2	2.36 ×2	2.41 ×2	2.44 ×2	2.54(1) ×2
			2.46 ×2	2.52 ×2	2.60 ×2	2.62 ×2	2.57(1) ×2
			2.92 ×2	2.82 ×2	2.75 ×2	2.78 ×2	2.69(1) ×2

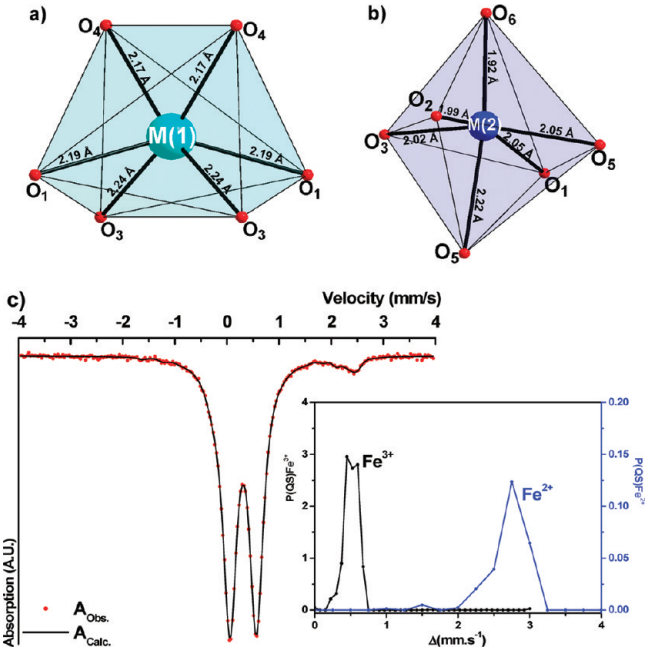

Figure 6. (a) $M(1)O_6$ and (b) $M(2)O_6$ octahedra. (c) Comparison of the experimental Mössbauer spectra of $NaMnFe_2(PO_4)_3$ collected at room temperature with the fitted one; the associated quadrupolar splitting distribution is also shown and the corresponding fitted parameters are given in Table 4.

Table 4. Mössbauer Fitted Parameters for $NaMnFe_2(PO_4)_3$ Prepared by Method B; Mössbauer Spectrum Was Recorded at 293 K

$NaMnFe_2(PO_4)_3$	*δ* (mm/s)	Δ (mm/s)	Γ (mm/s)	%	site
distribution 1	0.43	0.58	0.25	93	Fe^{3+} [Oh]
distribution 2	1.22	2.60	0.25	7	Fe^{2+} [Oh]

different octahedral sites: the major one (93%) is assigned to HS-Fe^{3+} and the minor one (7%) is assigned to HS-Fe^{2+}. Seven percent of the total number of iron ions correspond to the presence of 0.14 Fe^{2+} ions in the phase, which is on the same order of magnitude than the Fe ions quantity found in the M(1) site by neutron diffraction analysis, i.e., 0.13. We therefore assigned the Fe^{2+} Mössbauer signal to iron ions located in the M(1) octahedral sites. The presence of Fe^{2+} ions in the $NaMnFe_2(PO_4)_3$ phase implies the presence of some manganese ions exhibiting the Mn^{3+} oxidation state to maintain neutrality. To confirm the oxidation state of each atom, the bond valence sum has been calculated using the Brown method[32] for each transition metal in each site with the hypothesis of 2+ or 3+ oxidation states (Table 2). For M(1), the bond valence sum method is in good agreement with a 2+ oxidation state for both Mn and Fe ions, which reinforces our Mössbauer signals attribution. For M(2), the bond valence sum method is in good agreement with a 3+ oxidation state for Fe and Mn ions. Therefore, on the basis of our XRD and neutron diffraction study of $NaMnFe_2(PO_4)_3$, together with the results of Mössbauer spectroscopy and application of the bond valence sum method on M(1) and M(2) sites (Figure 6b, c), we suggest the following formulation for the phase prepared by method B: $(Na_{0.81})_{A(1)}(Na_{0.19})_{A(2)'}(Mn^{II}_{0.87}Fe^{II}_{0.13})_{M(1)}(Fe^{III}_{1.87}Mn^{III}_{0.13})_{M(2)}(PO_4)_3$.

Note that the phase prepared by method A was not analyzed by neutron diffraction to investigate a possible exchange between the M(1) and M(2) sites, but exhibits also 5% of Fe^{2+} ions from Mössbauer spectroscopy, suggesting that 0.1 Fe^{2+} would be exchanged with 0.1 Mn^{3+}.

In the literature, for $Na_{1.304}Mn_{0.968}Fe_{1.9}(PO_4)_3$, Hermann et al.[15] also observed Fe^{2+} ions by Mössbauer spectroscopy, but in a larger amount (~19%). Such differences can be understood by the fact that their structural composition differs significantly from ours, as it exhibits an excess of Na^+ ions, implying itself the presence of Fe^{2+} for charge compensation $(Na_{1+x}Mn^{II}Fe^{III}_{2-x}Fe^{II}_x(PO_4)_3)$. Moreover, the possibility for an exchange between the M(1) and M(2) sites has not been considered in their structural model.

As our material was prepared at 800 °C and quenched (method B), one can assume that at high temperature, there is a partial exchange between Fe and Mn ions in the two M sites. During the quenching procedure, a part of the disorder remains. Because the framework imposes the presence of two different types of sizes for the MO_6 octahedra, there is an internal redox process that minimizes the energy from the crystal field point of view. Therefore, one can consider that this disorder is certainly strongly related to the thermal treatment. The presence within the chains of both $Mn^{2+/3+}$ and $Fe^{2+/3+}$ redox

(32) Altermatt, D.; Brown, I. D. *Acta Crystallogr., Sect. B* **1985**, *41*, 240–244.

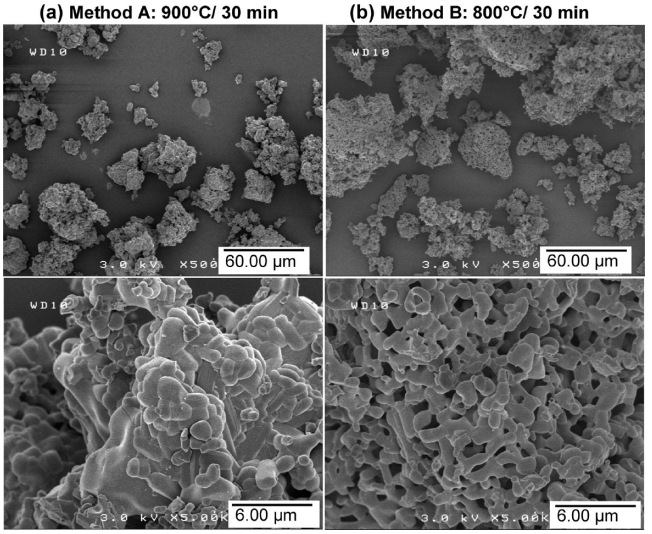

Figure 7. SEM micrographs showing the morphology and particle size of $NaMnFe_2(PO_4)_3$ powders prepared (a) by method A and (b) by method B.

couples has to be discussed in relation with the green color of the material: with such an electron distribution, black color was expected because of the possibility of electronic hopping. In this case, the green color shows that there is a strong electron localization due to the strong difference in crystal field between M(1) and M(2) sites. This behavior will have a considerable influence on the electrochemical properties, which will be further discussed.

3.2. Electrochemical Properties. The powder morphology for a positive electrode material is important because smaller grain size favors the intercalation process in the primary particles by reducing the ion-diffusion path length. We tried, thus, to decrease the particles size by preparing the $NaMnFe_2(PO_4)_3$ phase by method B (sol−gel method, 800 °C). In Figure 7, are compared the micrographs of the $NaMnFe_2(PO_4)_3$ samples prepared by methods A and B. The $NaMnFe_2(PO_4)_3$ sample prepared by method A exhibits compact aggregates (ranging between 15 and 50 μm in diameter), so dense that the primary particles are not clearly seen anymore. On the other hand, the $NaMnFe_2(PO_4)_3$ sample prepared by method B exhibits in average aggregates ranging between 10 and 60 μm in diameter with a spongy aspect and consisted of 1−3 μm primary particles. The spongy aggregates morphology of the phase obtained by method B is favorable for a better electrolyte impregnation. However, the primary particles remain pretty large and the synthesis could be further optimized.

$NaMnFe_2(PO_4)_3$ was tested as positive electrode in lithium cells. The cycling curves obtained for $NaMnFe_2(PO_4)_3$ prepared by the two methods, A and B, are given in Figure 8. Even if the two cells exhibit similar cycling profiles, much better performances are obtained for the cell with $NaMnFe_2(PO_4)_3$ prepared by method B: up to 1.5 Li^+ ions per formula unit could be intercalated during the first discharge with an average voltage around ~2.5 V and about 1.2 Li^+ ions could be extracted during the following charge (between 1.5 and 4.5 V vs Li^+/Li) with

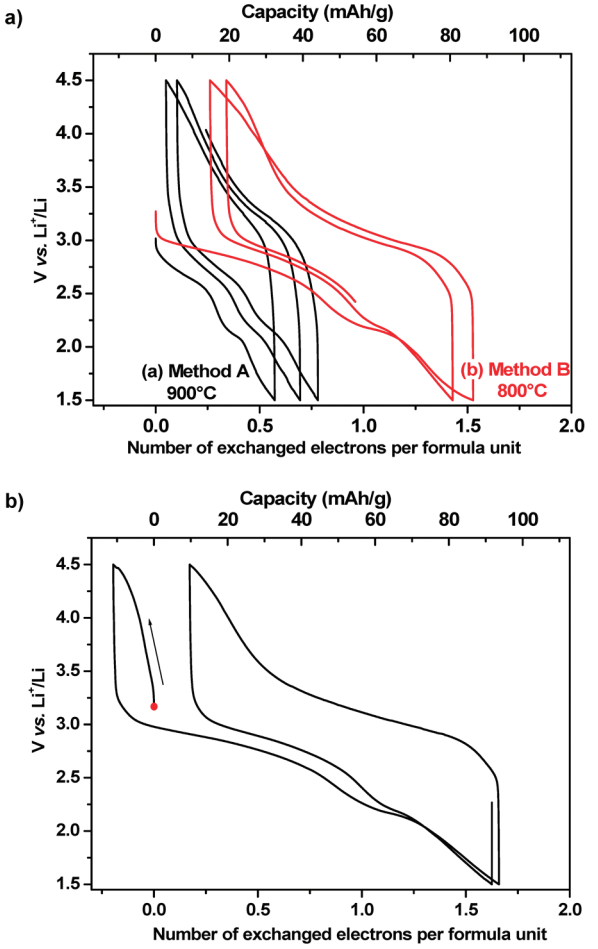

Figure 8. (a) Comparison between the electrochemical cycling curves of $Li//NaMnFe_2(PO_4)_3$ cells with $NaMnFe_2(PO_4)_3$ prepared by method A and method B, starting by a discharge of the cell ($C/50$ rate). (b) Cycling curve recorded for a $Li//NaMnFe_2(PO_4)_3$ prepared by method B cell, starting by a charge of the cell ($C/50$ rate).The red dot indicates the beginning of the cycling process.

an average voltage around ~3.2 V. A large irreversible capacity is thus observed. $Li//NaMnFe_2(PO_4)_3$ (method B) cells were also studied starting by a charge of the cell, i.e. removing some sodium ions. The corresponding cycling curve is given in Figure 8b. About 0.2 Na^+ ions could be removed from the structure up to 4.5 V vs Li^+/Li, associated to the oxidation of some Fe^{2+} and/or Mn^{2+} ions. After the first charge, the following discharge curve indicates that around 1.8 Li^+ ions per formula unit can be intercalated in the electrode material (corresponding capacity ~100 mAh/g). However, during the second charge, only 1.4 alkaline ions (Li^+ and/or Na^+) could be removed from the electrode material (corresponding capacity ~80 mA h/g). During the discharge, a voltage step is observed around 2.2 V that is not observed during the following charge. During cycling, this feature disappears progressiv, i.e., there is a change in the alkaline distribution within the framework. The cycling capacities achieved are slightly higher when the cell is first charged (some Na^+ ions first removed from the structure).

$NaMnFe_2(PO_4)_3$ materials prepared by methods A and B were also tested as positive electrode in sodium cells. The galvanostatic cycling curves starting by a charge of

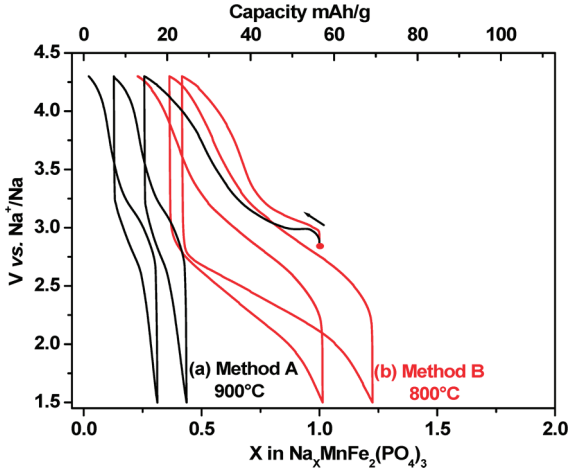

Figure 9. Comparison between the electrochemical cycling curves of $Na//NaMnFe_2(PO_4)_3$ cells with $NaMnFe_2(PO_4)_3$ prepared by method A and method B, starting by a charge of the cell ($C/100$ rate). The red dot indicates the beginning of the cycling process.

the cell are shown in Figure 9. It appears that $NaMnFe_2(PO_4)_3$ prepared by method A is really poorly electrochemically active in the 4.3−1.5 V vs Na^+/Na voltage range. $NaMnFe_2(PO_4)_3$ prepared by method B exhibits a better capacity however still pretty weak. Note that in this potential window the degradation of the sodium liquid electrolyte upon charge is important and leads to a strong shift of the curve toward low sodium concentration values. It is therefore difficult to deduce the actual amount of Na^+ ions that can be deintercalated during the first charge for comparison with the value obtained during the first charge in lithium cell. A detailed study of the structure evolution during the electrochemical cycling in a lithium and sodium batteries will be published elsewhere.

Conclusions

The structural characterization has shown the simultaneous presence of the $Mn^{2+/3+}$ and $Fe^{2+/3+}$ redox couples in the starting material. Nevertheless, its green color shows that the electronic hopping is impeded by strong octahedral distortion. Therefore, even if the alluaudite seems from the structural point of view interesting for alkaline metal intercalation/deintercalation, the very difficult electronic transfer seems to be a major drawback. Moreover, its 1D diffusion character tends also to make difficult the alkaline metal diffusion. To improve its performance, nanomaterials are thus certainly required. In our conditions, we did not succeed in obtaining very small primary particles, but the synthesis may be further optimized.

Acknowledgment. The authors thank ILL for the neutron diffraction experiment and especially Emmanuelle Suard, M3PEC for calculation facilities, Cathy Denage, Philippe Dagault, Laetitia Etienne, and Jérémy Humez for their technical assistance and Stanislas Pechev for fruitful discussions.